Tribology International 165 (2022) 107260

Contents lists available at ScienceDirect

Tribology International

journal homepage: www.elsevier.com/locate/triboint

Uncertainty-based comparison of conventional and surface topography-based methods for wear volume evaluation in pin-on-disc tribological test

Giacomo Maculotti [a,*], Edoardo Goti [b], Gianfranco Genta [a], Luigi Mazza [b], Maurizio Galetto [a]

[a] Department of Management and Production Engineering, Politecnico di Torino, Corso Duca degli Abruzzi 24, 10129 Turin, Italy
[b] Department of Mechanical and Aerospace Engineering, Politecnico di Torino, Corso Duca degli Abruzzi 24, 10129 Turin, Italy

ARTICLE INFO

Keywords:
Wear testing
Surface topography
Uncertainty
Pin-on-disc

ABSTRACT

Precise wear evaluation is essential to develop prediction models, applied to design materials, components and to optimise new manufacturing processes. Pin-on-disc is a widespread standardised conventional sliding wear test. Conventional characterisation of resulting wear exploits gravimetric or profilometric techniques. These have inadequate precision and accuracy for applications characterised by low-wear and uneven morphology and are being replaced with high-resolution and information-rich inspections to measure surface topography. Metrological characterisation of topography-based methods still lacks in literature, which prevents the performance comparison with conventional techniques. This paper develops a framework to evaluate topography-based methods' measurement uncertainty and compare methods' performances accordingly on experimental wear data on PTFE and Aluminium. Results show that topographic methods improve pin-on-disc characterisation's reliability.

1. Introduction

All the mechanical components in machines experience wear that, together with corrosion and fatigue failure, is one of the primary reasons for engineering systems malfunctions, reduced operational efficiency and components replacement [1].

Sliding wear is closely related to friction, which in turn affects the efficiency of machines, responsible for both energetic and economic losses related to maintenance and parts replacements. However, the impact of wear and friction goes far beyond mere cost reduction; the definitive improvement in energy efficiency and environmental footprint is also a stimulating goal for the industry. The study of wear phenomena and the quantification of the amount of wear play a crucial role in applying the modern principles of Industry 4.0 and circular economy, potentially to any industrial process. Huge efforts have been made to broaden the understanding of tribological problems to achieve a more profound knowledge of wear causes and phenomena to relieve its effect [2]. In this scenario, wear control is becoming an urgent need and the precise evaluation of wear damage is crucial to develop prediction models for components and systems design and to support industrial process optimisation [3].

Wear phenomena are complex to investigate. Thus, several standards and custom tribo-tests are currently exploited [4,5]. Identifying and quantifying the effect of each possible influence factor is, if ever possible, extremely demanding [5,6]; consequently, different types of tribo-tests include the ones most relevant, based on the specific purpose of the investigation. Model tests, because of the high reproducibility of test parameters and, hence, of the results, are the most widely used in laboratory studies and research for materials science, where comparative analysis of results in standard conditions are relevant. Model tests simplify the contact condition (including geometry) with respect to the application they are aimed at, thus limiting their representativeness of actual applications. However, their role in mechanics is crucial, for they provide guidelines for further experimental testing on components and in support of numerical investigations [7].

Amongst the other model tests, pin-on-disc is a well-established and widespread wear test for research purposes [4]. The test consists of applying a known force orthogonally to the surface of a rotating sample by means of a pin at a certain radius R from the rotation axis [8]. Fig. 1 shows the schematic of the test setup. The sample rotates for a certain number of cycles; wear is generated because of the interaction with the loaded pin against the disc.

The pin-on-disc method is extensively used in many leading research

* Corresponding author.
E-mail address: giacomo.maculotti@polito.it (G. Maculotti).

https://doi.org/10.1016/j.triboint.2021.107260
Received 5 August 2021; Received in revised form 31 August 2021; Accepted 2 September 2021
Available online 8 September 2021

Nomenclature

CS	contact stylus instrument (contact profilometer)
CSI	coherence scanning interferometer
d	pixel dimension
d_x	lateral sampling step along the x-axis
d_y	lateral sampling step along the y-axis
GPS	Geometrical Product Specifications
GUM	Guide to the expression of Uncertainty in Measurement
k	coverage factor (to calculate expanded uncertainty)
K	units conversion factor for the relative volume (area of the projected surface topography)
M	number of points in a measured profile
m_r	material ratio
MCs	Metrological Characteristics as per ISO 25178–600:2019
N	number of measured profiles
nx	number of measured pixels along the x-direction
ny	number of measured pixels along the y-direction
P	confidence level
$\overline{R}$	average radius of the circular wear track on the disc
R_j	measured radius of the circular wear track on the disc of the j-th position
R_{nom}	nominal radius of the circular wear track on the disc
ROI	region of interest
$\overline{S}$	average cross-section area of the wear track on the disc
S_j	cross-section area of the wear track on the disc at the j-th position
S_{mc}	inverse of the areal material ratio function
S_{mr}	areal material ratio function
$u(x)$	standard uncertainty for the x-axis
$u(y)$	standard uncertainty for the y-axis
$u(z)$	standard uncertainty for the z-axis
u2(g)	variance of the dependent quantity g
$u^2\left(\overline{V_{ISO}}\right)$	variance of the standardised volumetric method
$u^2\left(\overline{V_{ISO,R_{nom}}}\right)$	variance of the standardised volumetric method with nominal track radius
$u^2\left(\overline{V_{ISO,\overline{R}}}\right)$	variance of the standardised volumetric method with average track radius
$u^2\left(\overline{V_{prof,\ alt}}\right)$	variance of the alternative method to compute the mean wear volume
$u^2(V_{aut})$	variance of the automatic surface topography-based method
V_{aut}	volume measured on surface topography measurement by automatic function of commercial software
V_{damage}	volume corresponding to the total damage related to the mechanical interaction at the interface
$V_{galling}$	volume attributed to plastic flow or debris deposition
V_m	material volume
V_v	void volume
V_{VP}	volume measured on surface topography measurement by the surface topography parameter-based method
V_{wear}	volume attributed to material loss
$\overline{V_{ISO}}$	volume measured as per tribological standards (by 2D profilometry)
$\overline{V_{prof,\ alt}}$	volume measured through 2D profilometry with an alternative calculation method
x_i	coordinate of the measured point at the i-th sampling position along the x-axis
y_i	coordinate of the measured point at the i-th sampling position along the y-axis
z_i	value of profile or surface height at the i-th sampling position

fields thanks to its flexibility and simple setup and control of test parameters. The test is exploited to support aerospace [9], automotive and aeronautical applications of new low-density and high strength alloys [10], composite materials, e.g. Al-Metal Matrix Composites [11], and coatings [12]. Literature reports applications aimed to explore the tribological properties of innovative 2D-coatings, e.g. graphene and graphite-based coatings [13–15], to characterise green manufacturing processes, e.g. dry machining [16], to analyse the performance of coated tools [17,18], and to investigate the wear behaviour of components by additive manufacturing processes [19,20]. Also, lubricants and lubrication-related issues can be effectively investigated by pin-on-disc [21–24].

The measurement of the damage brought about by wear is the ultimate goal of any wear testing. Two standard techniques to measure wear in pin-on-disc tests are suggested by ASTM G99–17: precision weighing of samples (referred to as gravimetric method) and stylus-profilometry of the wear traces (referred to as volumetric method) [25]. However, technology offers today much more advanced and information-rich inspection techniques, featuring higher resolution and based on the measurement of surface topography. Nowadays, these methods are resorted to by an increasing number of laboratories because their cost has become affordable [26–36]. Nonetheless, tribological standards have not incorporated them yet, and a rigorous metrological characterisation, necessary to evaluate their uncertainties, is still lacking in the scientific literature.

This paper aims to develop a framework for evaluating the measurement uncertainty for surface-topography-based methods to enable and carry out a performance comparison with respect to the standardised approaches in quantifying wear in pin-on-disc tests. The authors have chosen to focus on the issues related to the measurement of disk wear, according to ASTM G99 that suggests reporting wear measurements separately for the pin and the disk, rather than as one value comprehensive of both contributions.

The paper is structured as follows. Section 2 discusses the state-of-the-art methods available in standards and the literature to evaluate the wear volume in a pin-on-disc test. Section 3 addresses the evaluation of measurement uncertainties for the procedures outlined in Section 2, formerly missing in the literature. Section 4 describes the experimental setup by which results are obtained. Section 5 discusses results: the evaluation in Section 3 enables performance comparison of the considered methods within a metrological framework. Section 6 finally draws conclusions.

2. Methods for wear quantification in pin-on-disc tribological test

It is worth to recall some exact terminology from ASTM G40 [37] and consider the outcome of a pin-on-disc test to outline some practical aspects related to the measurand identification for wear measurements in pin-on-disc tests:

- *Galling* = a form of surface damage arising between sliding solids, distinguished by macroscopic, usually localised, roughening, and the creation of protrusions above the original surface; it is characterised by plastic flow and may involve a material transfer.
- *Wear* = alteration of a solid surface by progressive loss or progressive displacement of material due to relative motion between that surface and a contacting substance or substances.

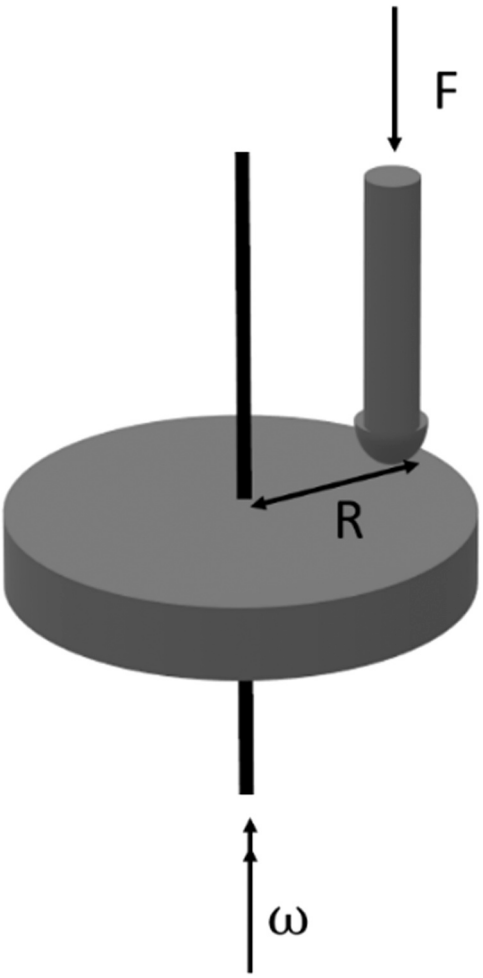

Fig. 1. Scheme of pin-on-disc. F is the applied force, on a rotating disc at speed ω, at a distance R from the rotation axis.

Fig. 2 shows the cross-section appearance of a typical disc wear track after a pin-on-disc test. It is straightforward to infer that the green part of the section above the reference line represents the volume attributed to either plastic flow or debris deposition, i.e. *galling*. On the other hand, the red region under the reference line is mainly the footprint left by material loss, i.e. *wear* according to the standard. While clear guidance is unreported in ASTM G99–17 on what after-tests measurements should cover, both wear and galling will be considered in this investigation, as well as the sum of these two quantities, which constitutes the (cumulative) surface *damage* due to mechanical actions:

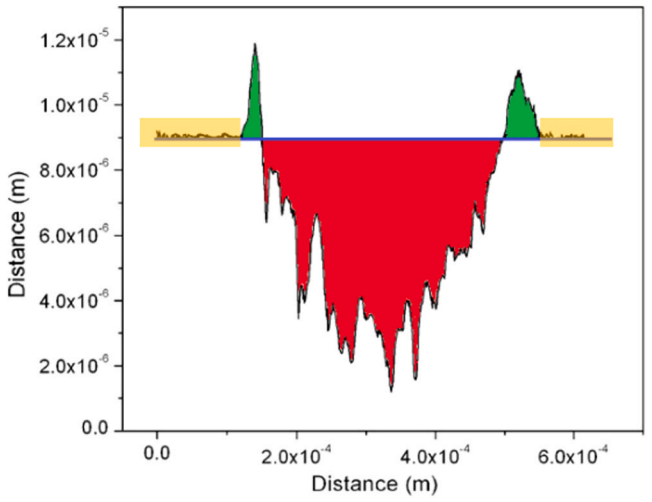

Fig. 2. Typical pin-on-disc wear track profile. In red, volume due to wear; in green, volume due to galling. The blue line is the reference to distinguish wear and galling; it is computed fitting profile in the yellow zones.

$$V_{damage} = V_{wear} + V_{galling} \tag{1}$$

Although some authors in the literature argue that while 'wear' is regarded as synonymous with material loss, material loss is only one facet of a more comprehensive definition of wear [38]. Any progressive change to a part involving relative motion with respect to another substance and that adversely affects its interface's performance should fall within the concept of wear [39]. In other words, wear is damage that seriously "disturbs" interface surfaces [42] and makes the contact loses its function [40,41].

As anticipated in the introduction, two standardised approaches are available to measure wear: the gravimetric and the volumetric approaches; they both achieve a characterisation of wear in terms of volume of material loss [25] but have very different descriptive qualities of the phenomenon.

The gravimetric approach achieves the estimation of wear by measuring the mass loss resulting from wear phenomena and is frequently used to measure wear because of the relative measurement simplicity [39]. However, it is insensible to damages related to plastic effects, and its result is altered by transferred material which binds to the surface and cannot be removed by simply cleaning the surfaces. Moreover, the gravimetric method is sensitive enough only if the wear is relatively large with respect to the mass of the body, thus being an inappropriate low-wear phenomenon analysis approach [39]. The resolution value of industrial precision balances is a percentage of their maximum capacity so that the required resolution cannot be easily achieved as the sample own weight would saturate the whole measuring capacity of the balance. Furthermore, to comply with the definition of wear, the measurand density must be known accurately, limiting the application of this method only to homogeneous materials with confidence [40]. In fact, multi-phase and layered materials may yield substantial errors in the estimation of wear since it is impossible to know the mass loss to be attributed to each phase separately [43,44]. As to coatings, density varies significantly according to the deposition method (due to porosity) and therefore may not be easily determined.

The volumetric approaches directly consider the volume of the surface damage as a measure of wear, with the measurand being the amount of material that has undergone modifications during the interaction (removed or displaced). The volumetric approaches are unaffected by the inhomogeneity of materials and can provide an accurate indication of wear in the presence of different phases. Moreover, these methods often can distinguish between the contribution coming from material displacement and material loss, and sometimes even between material loss and transfer phenomena [39]. Therefore, the volumetric methods are more flexible because they allow considering only the damage contribution relevant to the application. For instance, material loss is relevant when testing materials for brake pads or clutches. Conversely, the total damage may be preferred if the accumulation of transferred material on the surface is relevant, which is typical for applications where profile shape and tolerances are of paramount importance, e.g. in gears [45], couplings in general, and in the study of alteration of lubrication regimes by wear effects. Topography-based volumetric methods take further advantage by the reconstruction of worn surfaces, giving extended characterisations capabilities. The quantitative analysis is enriched with visual information on how the worn topography looks, which may definitively help recognise the various contributions to the total damage (loss, transfer, etc.).

In the following, the gravimetric method will be disregarded due to the above-mentioned limitations. The analysis will focus on the different interpretations of the volumetric method to assess the damage on the

disc resulting from a pin-on-disc test. These approaches, which can either rely upon standardised profilometric measurements or upon surface topography measurements, are discussed in the following sections and are preliminarily summarised in Table 1.

It is worth recalling here that pin-on-disc approach conventionality hinders its application if a significant amount of transferred material grows welded into the wear track [25]. In fact, in such cases, measurements (regardless if by gravimetric or volumetric methods) are affected by a non-quantifiable systematic error, limiting the method's representativeness [39]. The limitations of the gravimetric approach were formerly discussed. On the other hand, the volumetric method is unsuited if a third-body-based wear definition is considered [37]. In fact, the end-of-the-test wear tracks analysis alone would not provide any information on the volume of third-body particles ejected outside of the contact during the test [41] unless specific experimental protocols are established.

2.1. Standardised volumetric methods

According to ISO 18535:2016 [46] and ASTM G99–17 [25] the amount of disc wear resulting from a pin-on-disc test can be evaluated by Guldino's theorem:

$$V_{ISO} = \frac{2\pi}{N} R \sum_{j=1}^{N\geq 4} S_j \tag{2.1}$$

where R is the radius of the wear track and S_j the cross-section area of the wear track at the j-th location, see Fig. 3.

The standard volumetric method requires to extract N cross-section profiles; the wear track radius can be set to either the nominal track radius, R_{nom}, or the average radius of the extracted profiles, $\overline{R} = \frac{\sum_{j=1}^{N\geq 4} R_j}{N}$. Though, the standards do not specify which of the two is to prefer. Recalling that the profiles are heights z as a function of the lateral displacement, the lateral scanning along x-axis, $z(x)$ (as shown in Fig. 4a), one way to compute the cross-section area, S_j, is the rectangle method, depicted in Fig. 4b:

$$S_j = d_x \sum_{i=1}^{M} |z_i| \tag{2.2}$$

where M is the number of sampled points in the profile and d_x is the lateral sampling step, i.e. the lateral resolution along the x-axis.

The dependence on an average value in Eq. (2.1) is made explicit in Eq. (2.2), which points out that the standard volumetric method evaluates the average wear volume of the track because it considers the average cross-section area $\overline{S}$.

$$V_{ISO} = \frac{2\pi}{N} R \sum_{j=1}^{N\geq 4} S_j = 2\pi R \overline{S} = \overline{V_{ISO}} \tag{3}$$

The average volume evaluation is inherent in the definition and the limited representativeness of the approach. The extraction of few profiles, e.g. $N = 4$, cannot robustly represent the phenomenon when the track is highly irregular either along the circumferential wear path or across it. Colbert et al. [48] showed that, for reasonably regular tracks, a suggested threshold to reduce the approximation errors is $N = 8$.

An alternative to this method, hereby proposed, consists of considering the average of the volumes that would result considering N cross-sections and the corresponding apparent track radii R_j, rather than the mean volume evaluated by multiplying a given (nominal or average) track radius by the average cross-section:

$$\overline{V_{prof,\ alt}} = \frac{2\pi}{N} \sum_{j=1}^{N\geq 4} R_j S_j \tag{4}$$

All equations introduced thus far are general and refer to the evaluation of the V_{damage}, see Eq. (1). It is necessary to evaluate a reference line with respect to which to compute the heights and, most importantly, separate contributions for the computations to distinguish between volumes due to wear and galling. The reference line is typically computed by linearly least-square fitting the profile heights outside a specific region of interest of the profile, e.g. the unworn yellow regions in Fig. 2.

Even though standards are conceived for the application of the volumetric methods by contact stylus (CS) instruments, e.g. contact profilometers, literature reports several implementations of the standard volumetric methods based on surface topography measurements, e.g. coherence scanning interferometers (CSI), confocal microscopes (CM) by the software extraction of profiles from the measured surface [26,28–30,32,48–50].

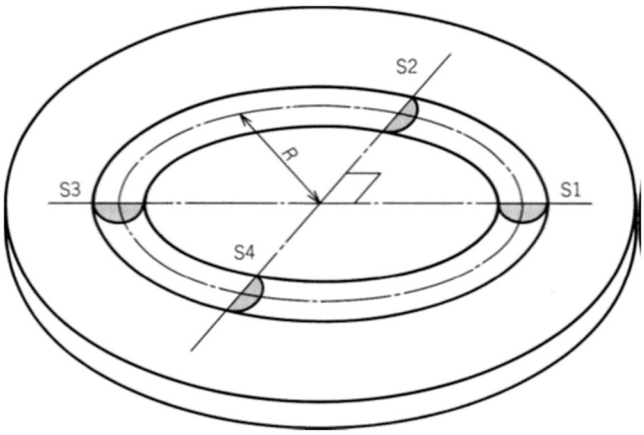

Fig. 3. Scheme of volumetric wear measurement as per ISO 18535:2016.

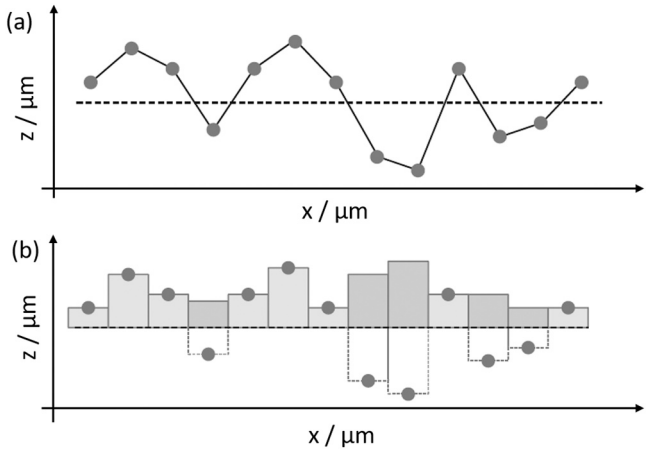

Fig. 4. (a) profile heights z as function of lateral scanning step x. (b) rectangle method for area evaluation.
Adapted from [47].

Table 1
Considered methods for volumetric wear measurement in this paper.

Measurement method	Profilometry		Surface topography	
Method interpretation	As per standard	Alternative	Automatic	Parameter-based
Symbol used	$\overline{V_{ISO}}$	$\overline{V_{prof,\ alt}}$	V_{aut}	V_{VP}

2.2. Volumetric methods based on surface topography measurements

The application of areal-topography measurement methods to simply extract profiles generates a significant data loss and yields no significant practical advantages in representativeness [51]. As pointed out in the former subsection, volumetric methods based on profiles allows evaluating the mean wear volume only. Therefore, the latest scientific literature reports introducing methods that fully exploit topography for wear volume characterisation.

Two main approaches can be distinguished: a numerical one, which still relies upon profile extraction, and an alternate one based on surface texture parameters.

In both cases, some preliminary operations are necessary. First, standard S- and F-operators to get the scale-limited S-F surface must be applied [52,53], i.e. the surface after the removal of the noise content and the underlying shape; then the identification of the wear track should be carried out to extract a region of interest (ROI). The track identification can either be done manually or by exploiting segmentation methods [44]. The extraction of the ROI is necessary to exclude from the following computations the effect of roughness and topographical features that are not related to the tribological test. Even if extremely computationally demanding, an effective way consists of measuring the tested surface before and after the test and evaluating the worn surface by subtraction of the two, provided a preliminary registration step of the two measurements [33,54–57].

The first topographical method herein described is entirely automatic; it is implemented in several commercial software for surface topography characterisation, e.g. MountainsMap®. It requires to extract a series of several (N) profiles $z(x)$ along the direction orthogonal to the profile scanning, i.e. the y-axis being the x-axis the profile scanning direction, and to compute the (total) damage volume as:

$$V_{aut} = d_y \sum_{j=2}^{N-1} S_j + \frac{d_y}{2}(S_1 + S_N) \tag{5}$$

where d_y is the sampling distance along the y-axis [49,58,59] and S_j is the cross-section area, defined in Eq. (3). The evaluation of a reference surface height by plane-least square fitting of the topography outside the ROI allows distinguishing between the wear and galling contribution to the damage.

The second approach is based on volume parameters [47,60,61] and allows to compute the total damage as:

$$V_{VP} = V_m(m_r) + V_v(m_r) \tag{6.1}$$

$$V_m(m_r) = K \int_{0\%}^{m_r} (S_{mc}(p) - S_{mc}(m_r)) \, dp \tag{6.2}$$

$$V_v(m_r) = K \int_{m_r}^{100\%} (S_{mc}(m_r) - S_{mc}(p)) \, dp \tag{6.3}$$

where, V_{VP} is the damage volume evaluated as per the volume parameters topographic method, V_m and V_v are the material volume and the void volume, respectively. S_{mc} is the inverse of the areal material ratio function (S_{mr}), i.e. the cumulative probability distribution of the surface heights. K is a factor to convert the relative volume into the most appropriate unit and represents the area of the projected surface topography on a horizontal plane. Given a specific horizontal section plane whose height is $h_0 = S_{mc}(m_r)$, V_m represents the volume of material enclosed below the measured surface and above this plane, whilst V_v is the volume of missing material above the surface and below this plane. Fig. 5 represents these two parameters graphically in relationship to the S_{mr} curve.

Here, the relevance of appropriately choosing the reference height, m_r, is even more apparent, and the Abbott-Firestone curve is an effective tool to identify it. Therefore, the following relationship between Eqs. (1) and (6) can be stated:

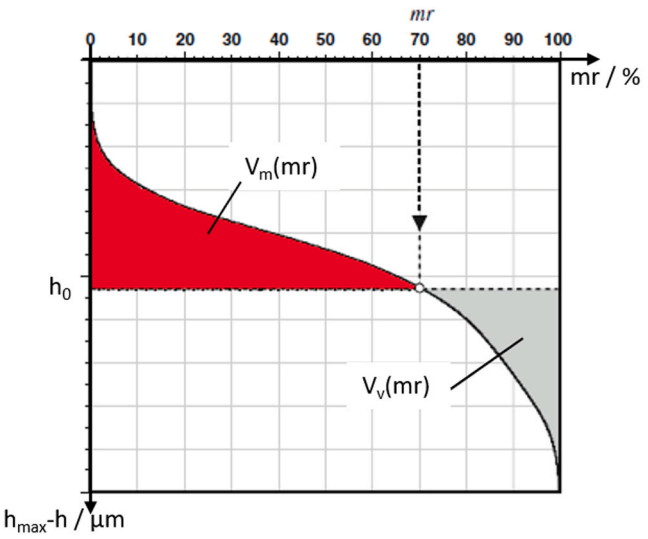

Fig. 5. Void and Material volume parameters
Adapted from [52].

$$\left\{ \begin{array}{l} V_{galling} = V_m(m_r) \\ V_{wear} = V_v(m_r) \end{array} \right\} \tag{7}$$

3. Uncertainty evaluation of volumetric wear measurements

Evaluating the different volumetric wear measurement methods' measurement uncertainty is necessary to enable the methods' performance comparison. The *Guide to the expression of uncertainty in measurement* (GUM) [62] establishes the methods for computing it. In the case a known mathematical model can be explicitly written between the measurand (dependent) quantity g and the independent quantity $\boldsymbol{x}$, the former can be written as:

$$G = f(\boldsymbol{X}), \quad G \in \mathbb{R}^1, \boldsymbol{X} \in \mathbb{R}^{n,1} \tag{8}$$

If this model is linearisable, the variance of the dependent quantity $u^2(g)$ can be computed according to the equation:

$$u^2(g) = \boldsymbol{c}^T \boldsymbol{VCV} \boldsymbol{c} = \sum_{a=1}^{n} \sum_{b=1}^{n} c_a c_b VCV_{ab} \tag{9}$$

where $\boldsymbol{c} \in \mathbb{R}^{n,1}$ is the vector of sensitivity coefficients, i.e. the partial derivatives, so that $c_a = \frac{\partial f}{\partial x_a}$ and $\boldsymbol{VCV} \in \mathbb{R}^{n,n}$ is the variance-covariance matrix of the independent quantities, where $VCV_{ab} = Cov(x_a, x_b)$. Eq. (9) is the law of uncertainty propagation, which is a particular case of the law of variance propagation. In the case of uncorrelated independent quantities, Eq. (9) can be rewritten as:

$$u^2(g) = \sum_{a=1}^{n} \left(\frac{\partial f}{\partial x_a} \right)^2 u^2(x_a) = \sum_{a=1}^{n} u_a^2(g) \tag{10}$$

where $u^2(x_a)$ is the variance of the a-th influence factor and can be either statistically or non-statistically evaluated, depending on whether it is a type A contribution or a type B contribution, respectively.

It is reasonable in most practical cases to assume that G distributes normally, i.e. $G \sim N(\mathbb{E}[G], \mathbb{V}ar[G])$. Its (expanded) uncertainty $U(g)$ is:

$$U(g) = k \bullet \mathrm{u(g)} \tag{11.1}$$

$$k = t_{\nu,\ P}^{-1} \tag{11.2}$$

$$\nu = \left\lfloor \frac{u^4(g)}{\sum \frac{u_a^4(g)}{\nu_a}} \right\rfloor \tag{11.3}$$

where k is the coverage factor computed as the quantile of a *t-Student* distribution with ν degrees of freedom at a certain confidence interval P. The degrees of freedom are computed according to the Welch-Satterthwaite formula in Eq. (11.3) as a function of the degrees of freedom with whom each individual contribution is estimated.

In the following, results will be provided in terms of variances for the sake of compactness.

In literature, despite the common application of volumetric methods to assess wear in pin-on-disc test, measurement uncertainty evaluations are either unreported, as in the case of surface topography-base methods, or do not rely upon ISO 25178–600:2019 [63], the latest standard for surface topography measuring instruments belonging to the Geometrical Product Specifications (GPS) framework. This standard introduces the concept of Metrological Characteristics (MCs), i.e. *characteristics of the measuring equipment, which may influence the result of measurement, may require calibration and have an immediate contribution to measurement uncertainty*.

The measurement uncertainty of a surface inspection instrument is influenced by several factors, such as environmental, mechanical and electrical noise, optical aberrations and mathematical algorithms. Assessing the contribution of each individual factor would be time-consuming and often unnecessary for the end-user. Thus, an input-output model has been introduced to account for the influence factors by few synthetic indicators [64], i.e. the MCs. These are seven and can be traced back to the typical measurement error contribution listed in Table 2.

The methods to evaluate the MCs have been defined by Giusca and colleagues [65–67], with the sole exception of T_{FI} that is still unreported [68]. They are applied for several technologies, e.g. CS, CSI and CM [65–67], focus variation microscopes [69,70] and point autofocus instruments [71,72]. According to their definition, MCs directly contribute to the measurement uncertainty. The resulting standard uncertainties are summarised in Table 3 and are combined as standard uncertainties of the axes as in Eq. (12) [65–67].

$$u(z) = \sqrt{u_{N_M}^2 + u_{z_{FLT}}^2 + u_z^2 + u_{T_{FI}}^2} \tag{12.1}$$

$$u(x) = \sqrt{u_{W_R}^2 + u_x^2} \tag{12.2}$$

$$u(y) = \sqrt{u_{W_R}^2 + u_y^2} \tag{12.3}$$

Table 2
ISO 25178–600:2019 Metrological Characteristics of surface topography measuring instruments.

Metrological characteristic	Symbol	Main potential error direction	Error type
Amplification coefficient	α_x, α_y, α_z,	*x*, *y*, *z*	Systematic
Linearity deviation	l_x, l_y, l_z,	*x*, *y*, *z*	Systematic
Flatness deviation	z_{FLT}	*z*	Reproducibility and systematic error due to system reference
Measurement noise	N_M	*z*	Repeatability
Topographic spatial resolution	W_R	*z*	Resolution
x-y mapping deviation	$\Delta_x(x,y)$, $\Delta_y(x,y)$	*x*, *y*	Systematic
Topography fidelity	T_{FI}	*x*, *y*, *z*	Systematic

Colbert et al. [48] developed the computation for the wear volume measurement according to the standard. However, in their paper, the metrological characteristics of the measuring instruments were not considered. According to the current standard framework of ISO 25178, MCs are supposed to support and simplify the propagation of the measurement uncertainty; therefore, the computation by Colbert will be revised in paragraph 3.1 to comply with ISO 25178 in the hypothesis of uncorrelated independent variables. Moreover, evaluating the measurement uncertainty for the surface topography-based methods, which is still lacking in the literature, will be formulated within this same framework in the following paragraphs. Influence factors will be discussed and final results reported; computation details are reported for readability in Annex A.

3.1. Standard method

Recombining Eqs. (2.1) and (3), it follows:

$$\overline{V_{ISO}} = \frac{2\pi}{N} d_x R \sum_{j=1}^{N\geq 4} \sum_{i=1}^{M} |z_{ji}| \tag{13}$$

that highlights the measured independent quantities. These are summarised in Table 4, which also reports their variability contribution, i.e. their measurement uncertainties evaluated according to Eq.(11) to cater for the metrological characteristics.

The variance due to the pixel size, d, according to Giusca and Leach [67], can be associated with a triangular distribution with half-range d so that $u^2(d) = \frac{d^2}{6}$. The contribution $u(R)$ due to the track radius R depends on the choice of R between R_{nom} and $\overline{R}$. In the first case, $u(R_{nom})$ can be estimated according to the P.U.Ma. method as two units of the Least Significant Digit (*LSD*) of the mean value, $2 \bullet LSD$, and associating to this half range of a uniform distribution [62]; otherwise, the law of variance propagation is required to be invoked, proceeding based on the definition of $\overline{R} = \frac{\sum_j^{N\geq 4} R_j}{N}$.

The variance of the standardised volumetric method for the mean wear volume measurement can be computed taking into account its definition in Eq. (2.2) and the contribution from the area of the average cross-section and the track radius, for which two alternatives are possible:

$$u^2\left(\overline{V_{ISO}}\right) = 4\pi^2 \left(\overline{S}^2 u^2(R) + \quad R^2 u^2\left(\overline{S}\right)\right) \tag{14}$$

which can be rewritten by outlining the two possible ways of handling R explicitly:

$$u^2\left(\overline{V_{ISO,R_{nom}}}\right) = 4\pi^2 \left(\overline{S}^2 u^2(R_{nom}) + \quad {R_{nom}}^2 \frac{\mathbb{E}\left[u^2\left(S_j\right)\right]}{N}\right) \tag{15}$$

$$u^2\left(\overline{V_{ISO,\overline{R}}}\right) = \frac{4\pi^2}{N} \left(\overline{S}^2 \mathbb{E}\left[u^2\left(R_j\right)\right] + \quad \overline{R}^2 \mathbb{E}\left[u^2\left(S_j\right)\right]\right) \tag{16}$$

3.2. Alternative method based on profile extraction

As discussed in Section 3.1, a possible alternative to the computation of the mean wear volume based on the average cross-section consists of averaging the volumes resulting when considering N cross-sections and their corresponding track radii per Eq. (4). $\overline{V_{prof,alt}}$ can be simplified as:

$$\overline{V_{prof,alt}} = \frac{2\pi}{N} \sum_j^{N\geq 4} R_j S_j = 2\pi \overline{RS} \tag{17}$$

The evaluation of the variance of the mean volume exploits previous intermediate computations carried out to obtain Eq. (14) in Section 4.1 and reported in Annex A.1, being the influence factors R_j and S_j defined in the same way, from which $u^2\left(\overline{RS}\right)$ is computed, that allows writing the wanted result:

Table 3
Contribution to measurement uncertainties of the metrological characteristics; α and Δ are not present as they contribute to define l and their contribution is there included [66].

Metrological characteristic	Distribution of the MC	Contribution to uncertainty
N_M	Normal	$u_{N_M} = N_M$
z_{FLT}	Uniform	$u_{z_{FLT}} = \frac{z_{FLT}}{\sqrt{12}}$
$l_{x,\ y,\ z}$	Normal	$u_{x,\ y,\ z} = \sqrt{\frac{l_{x,\ y,\ z}^2}{3} + u_{reproducibility_i}{}^2 + u_{repeatability_i}{}^2 + u_{ti}{}^2}$
W_R	Uniform	$u_{W_R} = \frac{W_R}{\sqrt{3}}$
T_{FI}	Normal	$u_{T_{FI}} = T_{FI}$

Table 4
Influence factors to standardised wear volume evaluation.

Influence factor	Measured quantity	Standard uncertainty
S_j	d_x	$u(d)$
	z_{ij}	$u(z)$
R	R	$u(R)$

$$u^2\left(\overline{V_{prof,\ \ alt}}\right) = 4\pi^2 u^2\left(\overline{RS}\right) = 4\pi^2 \frac{\mathbb{E}\left[u^2\left(R_j S_j\right)\right]}{N} \tag{18}$$

3.3. Automatic surface topography-based method

Although the scientific literature reports several applications of this method recently, to the authors' best knowledge, no method for estimating its measurement uncertainty has been formulated so far.

The definition in Eq. (5) highlights the influence factors, which are summarised in Table 5.

Thus, the variance computation is carried out through the law of uncertainty propagation and relies on the evaluation of $u^2(S_j)$:

$$u^2(V_{aut}) = \frac{d_y^2}{4}\left(u^2(S_1) + u^2(S_N)\right) + d_y^2 \times \sum_{j=2}^{N-1} u^2(S_j) \quad + \left(\sum_{j=2}^{N-1} S_j + \frac{S_1 + S_N}{2}\right)^2 u^2(d) \tag{19}$$

It is mandatory to derive the uncertainty of the mean volume to compare this method with the standard one consistently. This can be done by exploiting the variance of the sample mean, considering that the sample includes N extracted profiles:

$$u^2\left(\overline{V_{aut}}\right) = \frac{u^2(V_{aut})}{N} \tag{20}$$

3.4. Volume parameter method

The measurement uncertainty for volume parameters is unreported in literature, to the best knowledge of the authors. This evaluation requires to move from the continuous definition, as in Section 3.2, to the discrete one:

$$V_m(m_r) = \quad K\int_{0\%}^{mr}\left(S_{mc}(p) - S_{mc}(mr)\quad\right)dp \approx K\sum_{j=1}^{B}\Delta z_j m_{rj} \tag{21.1}$$

Table 5
Influence factors to automatic wear volume evaluation based on surface topography.

Influence factor	Measured quantity	Standard uncertainty
S_j	d_x	$u(d)$
	z_{ij}	$u(z)$
d_y	d_y	$u(d)$

$$V_v(m_r) = K\int_{mr}^{100\%}\left(S_{mc}(mr) - S_{mc}(p)\right)\quad dp \approx K\left(100\%(z_{max} - h) - \sum_{j=B+1}^{N_{bin}}\Delta z_j\ m_{rj}\right) \tag{21.2}$$

$$K = n_x n_y d^2 \tag{21.3}$$

where $h = S_{mc}(m_r)$, n_x and n_y are the number of measured pixels along the x- and y-axis, respectively, d is the pixel dimension in the hypothesis that $d_x = d_y = d$. It is necessary to approximate the material ratio curve by a histogram to work into the discrete domain. The histogram has N_{bin} bins so that h belongs to the B-th bin; the j-th bin is wide Δz_j and is associated with a material ratio of m_{rj}.

Under the assumption that the material ratio curve is computed exactly, i.e. the histogram is built exactly, m_{rj} does not contribute to the measurement uncertainty and the only influence factors are the height and the pixel width, as summarised in Table 6.

The variance of V_m, i.e. the $V_{gallling}$, V_v, i.e. the V_{wear}, and of the volume of the total damage are computed, applying the law of variance propagation:

$$u^2(V_m(m_r)) = \left(\sum_{j=1}^{B}\Delta z_j m_{rj}\right)^2 u^2(K) + 2K^2\sum_{j=1}^{B} m_{rj}^2 u^2(z) \tag{22.1}$$

$$u^2(V_v(m_r)) = \left((z_{max} - h) - \sum_{j=B+1}^{N_{bin}}\Delta z_j m_{rj}\right)^2 u^2(K) + 2K^2\left(1 + \sum_{j=B+1}^{N_{bin}} m_{rj}^2\right)u^2(z) \tag{22.2}$$

$$u^2(V_{VP}) = \left[\left(\frac{V_m(m_r)}{K}\right)^2 + \left(\frac{V_v(m_r)}{K}\right)^2\right]u^2(K) + 2K^2\left[1 + \sum_{j=1}^{N_{bin}} m_{rj}^2\right]u^2(z) \tag{22.3}$$

The variances of the mean volumes are now computed to compare with standard methods, as:

$$u^2\left(\overline{V_{galling}}\right) = \frac{u^2(V_m(m_r))}{n_x n_y} \tag{23.1}$$

$$u^2\left(\overline{V_{wear}}\right) = \frac{u^2(V_v(m_r))}{n_x n_y} \tag{23.1}$$

Table 6
Influence factors to wear volume evaluation based on volume areal field parameters.

Influence factor	Measured quantity	Standard uncertainty
Δz_j	z_i-z_j	$\sqrt{2}$•u(z)
h	h	$u(z)$
K	d	$u(d)$

$$u^2\left(\overline{V_{damage}}\right) = \frac{u^2(V_{VP})}{n_x n_y} \tag{23.1}$$

4. Materials and methods

The theoretical framework, formerly introduced, was applied to a simple case study to assess the performances of the available methods in estimating the wear volume in pin-on-disc tests. Tribological tests were performed using an Anton Paar TRB pin-on-disc tribometer (Laboratory of Mechanics, Politecnico di Torino, Italy). An Al-alloy sample and a PTFE sample were tested against an AISI 52100 (UNI 100Cr6) 6 mm diameter steel ball to generate wear tracks with different features and shape in similar testing conditions. One test with the same total sliding distance of 50 m was performed on each sample under 5 N load and linear speed of 0.05 m/s; the wear track radius was kept unchanged to ensure that the observed tribological phenomena are fully comparable, $R_{nom} = 5$ mm. Only one test per sample was deemed sufficient as the focus of this research work is on the wear volume measurement itself rather than its tribological meaning. Wear data from the pin-on-disc test with PTFE and Al-alloy are presented here with the purpose to exemplify two typical and extremely different worn region morphologies any researcher applying the pin-on-disc method may face with. The deep analysis of the wear mechanisms with these two materials under the specific testing conditions is beyond this investigation's purpose, except that very different topographic features appear against the same counterpart. The topographic appearance may indeed affect the relative difference in the accuracy of the wear volume measurements.

Fig. 6 shows the schematic of the pin-on-disc layout and the appearance of the surface damage on the two samples at the end of the tests. Aluminium is chemically compatible with steel and is expected to generate large debris due to strong adhesion. The test with this material shows a highly irregular track with deep valleys at a location where large chunks of material are released and mountains due to the localised plastic effect. On the contrary, PTFE typically features a smooth regular track against steel due to diffused ploughing effects with abrasive wear and limited galling at the wear track boundaries.

Both samples were ground and polished before the test to improve the surface finish. Table 7 summarises the main topographical and mechanical properties of samples and ball material.

At the end of the test, the samples were accurately cleaned with acetone to remove wear debris, and wear tracks were inspected to measure the surface damage volume. The wear damage on the spheric counterpart is negligible in this study because of the considered case studies. Similarly, the wear rate was not considered because the wear amount is the one quantity directly measured.

Wear, galling and total damage volumes are measured exploiting the equations formerly introduced by considering 4 and 8 profiles for the methods based on profile measurements (this is to test the consistency of these results with previous literature [48]). Moreover, profile measurements were considered directly measured by a contact stylus (CS), an SM Instruments RTP-80, and extracted from a surface topography measurement performed by a coherence scanning interferometer (CSI), a Zygo NewView 9000. This instrument was also employed to apply the methods based on surface topography. Measurements by the CS were performed at the lowest speed, i.e. 0.5 mm/s; the vertical and the lateral resolution of the CS are 1 nm and 6.25 μm, respectively, and the tip is a

Table 7
Mechanical properties of tested samples and testing sphere. For the samples, λs is 1 μm, and the F-operator is a 2nd order polynomial, to eliminate shape introduced by manual polishing; for the ball, λs is 2.5 μm and the F-operator a least-square fitted sphere [53]. Vickers scales have been chosen to test the same depth scale of the worn material during the pin-on-disc test, i.e., indentation depth is similar to the wear track's depth; ball hardness specified by the manufacturer.

Material	S_a / μm	S_q / μm	Hardness
AISI 52100 (ball)	0.13	0.22	60 HRC
Aluminium (sample)	0.31	0.40	76.89 HV 0.2
PTFE (sample)	0.34	0.48	2.95 HV 0.025

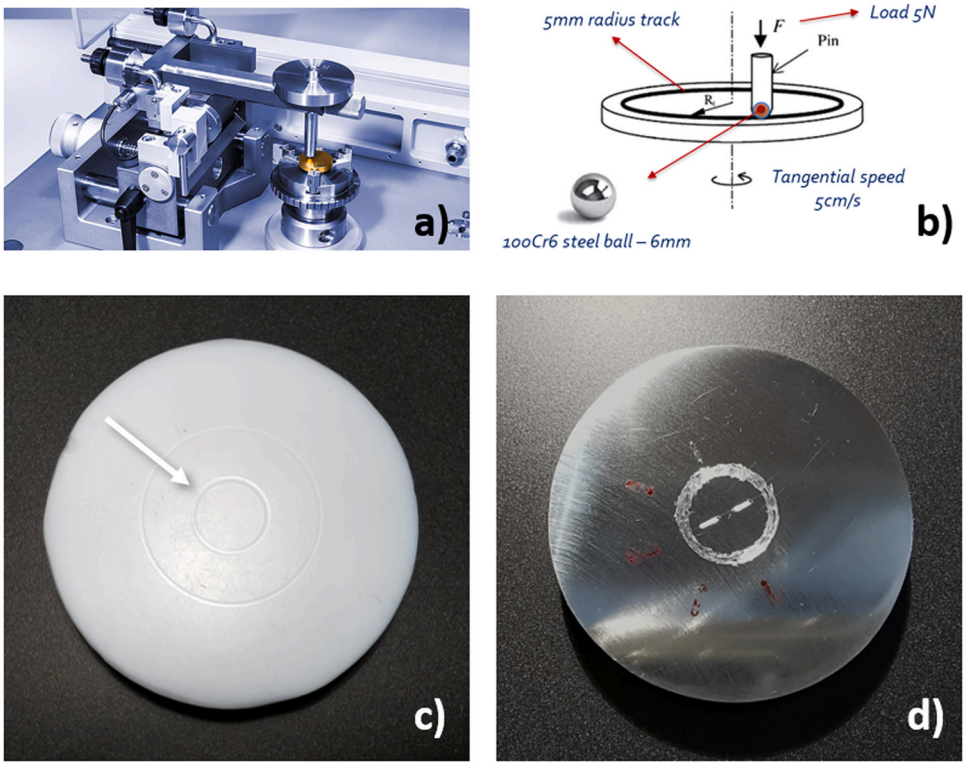

Fig. 6. (a) Anton Paar TRB pin-on-disc tribometer at Laboratory of Mechanics; (b) the pin-on-disc testing layout; (c) wear track on the PTFE sample; (d) wear track appearance on the aluminium sample.

standardised conical tip with a radius of 2 μm and cone angle of 90°. In the CSI case, two different measurement objectives were used to account for a possible effect of the lateral resolution: a Michelson 5.5×, with the numerical aperture of 0.15 and pixel size d of 1.56 μm and a Mirau 20× with a digital zoom at 0.5× with a numerical aperture of 0.4 and d of 0.87 μm. In both cases, stitching of several fields of view was necessary. The main benefit from the lower magnification is reducing the measurement time (about 15' and 30' respectively).

The overview of the experimental setups and the volume measurement methods are summarised in Tables 8 and 9.

Both instruments are hosted in the Technological Surface Metrology Laboratory at Politecnico di Torino, Italy. The contributions to the measurement uncertainty of their metrological characteristics are summarised in Table 10, estimated as type B contribution from the literature [65,66,73], and combined according to Eq.(12), yielding the values in Table 11.

Systematic differences amongst the methods in terms of their capability of estimating the average volume will be assessed by performing a hypothesis t-test at a confidence level of 95% on the difference of sample averages built as follow, considering two different average volume estimation by two different methods, i.e. $\overline{V_{M1}}$ and $\overline{V_{M2}}$, each related to a standard uncertainty $u\left(\overline{V_{M1}}\right)$ and $u\left(\overline{V_{M2}}\right)$:

$$H_0: \overline{V_{M1}} - \overline{V_{M2}} = 0$$

$$H_1: \overline{V_{M1}} - \overline{V_{M2}} \neq 0$$

At a confidence level p of 95%, the null hypothesis H_0 is rejected if

$$\left(\overline{V_{M1}} - \overline{V_{M2}}\right) \notin \left[t_{0.025,30}s; t_{0.975,30}s\right],$$

with $s = u\left(\overline{V_{M1}} - \overline{V_{M2}}\right) = \sqrt{u^2\left(\overline{V_{M1}}\right) + u^2\left(\overline{V_{M2}}\right)}$ and the coverage factor evaluated with 30 degrees of freedom according to the P.U.Ma method [62].

The same results can be obtained qualitatively by comparing the uncertainties bar: a systematic difference can be highlighted if they do not overlap. The surface topography-based methods are considered the benchmark to compare the other results: although they are nonstandard methods, the measuring methods' greater representativeness provide the necessary confidence to support this choice. For their application, ROIs were extracted manually as the measured region hindered automatic identification techniques because of computational limits.

5. Results discussion

Fig. 7 shows the surface topographies of the two samples. As intended, PTFE is characterised by a smooth and regular wear track, whilst Aluminium is highly uneven in-depth and shows craters and attached particles inside the track and severe galling at the edges. The black lines outline the cutting planes along which profile extraction was performed. Fig. 8 shows some examples of the pair of extracted profiles on both samples.

The comparison of the methods is reported in Figs. 9 and 10, which show the total damage volume for PTFE and Aluminium, respectively. Error bars represent the expanded uncertainty at a confidence level of 95% and 30 degrees of freedom, i.e. $k = 2$.

The diagrams of total damage volumes show that no significant differences in accuracy exist for regular tracks, and differences among the average values are within 5%, as is the case with PTFE [74]. Profile methods improve their precision by increasing the number of measured or extracted profiles, consistently with the average volume computation and with the literature [48]. Surface topography-based methods are inherently the best choice for precision (expanded uncertainty smaller than 1%).

In the case of Aluminium, characterised by a highly irregular track, the application of the standard profilometric methods based on very few extracted profiles shows poor accuracy. The surface topography-based methods are herein regarded as the most accurate, considering the greater representativeness of these measurements [52]. In some cases, the differences between the average values are up to 60% but improve by increasing the number of sampled profiles (again following [48]) [74]. The actual measurement of profiles by stylus profilometry (CS) significantly improves the accuracy; however, this effect can be ascribed to the worst lateral resolution, which tends to overestimate areas. Fig. 11 provides a graphical depiction of this effect: that the approximation of the sampled signal by the blue rectangles is worse than by the yellow ones.

Analysing the wear and galling volumes separately allows obtaining more insights into the performances. The wear volume measurement results are shown in Figs. 12 and 13 for the two samples, and similarly galling volumes in Figs. 14 and 15. For a regular wear track, in which wear is dominant over galling (V_{wear} is 95% of the V_{damage}), the accuracy amongst the methods is still acceptable in terms of volume of worn-out material (differences are within 5%) [74]. However, profiles methods tend to overestimate wear slightly and underestimate the contribution due to galling significantly and systematically. This issue is due to the lower representativeness of the profile methods, limiting their capability to measure a small and localised phenomenon, as galling is in the PTFE case. Conversely, a severe underestimation of the wear volume results in

Table 8
Measurement setup for the comparison of wear volume measurement method based on profile.

Profile-based method	Standard				Alternative	
R measurement	R_{nom}		$\overline{R}$		R_j	
Number of profiles (N)	4	8	4	8	4	8
Instrument setup	CS, CSI 5.5 × , CSI 20 ×					

Table 9
Measurement setup for the comparison of wear volume measurement method based on surface topography.

Surface topography-based method	Automatic (MountainsMap®)	Volume parameters
Instrument setup	CSI 5.5×, CSI 20×	

Table 10
Contribution to measurement uncertainties of metrological characteristics of considered instruments; u_{NF} includes both u_{N_M} and $u_{z_{FLT}}$ [65].

	CS	CSI
u_{NF} / nm	35	1
u_x / nm	400	100
u_y / nm	400	100
u_z / nm	5	10
u_{WR} / nm	3608	902 (5.5×) 600 (20×)

Table 11
Measurement uncertainty along the measuring axes of the considered instruments.

	CS	CSI	
		5.5×	20×
$u(x)$ / nm	3630	908	608
$u(y)$ / nm	3630	908	608
$u(z)$ / nm	35	10	10

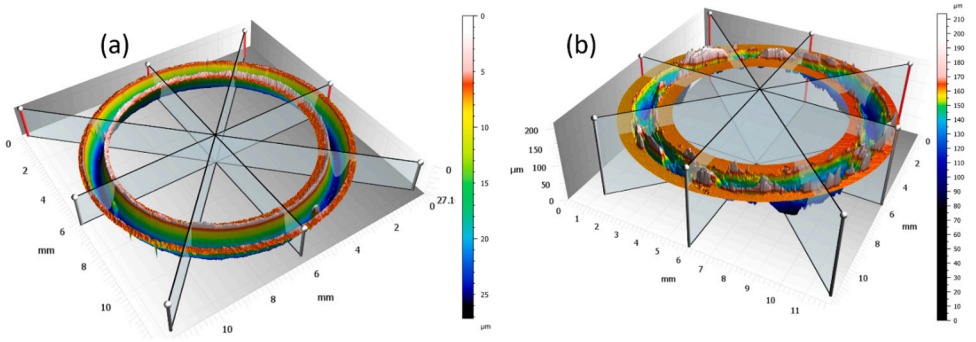

Fig. 7. Wear tracks of (a) PTFE and (b) Aluminium, measured with CSI.

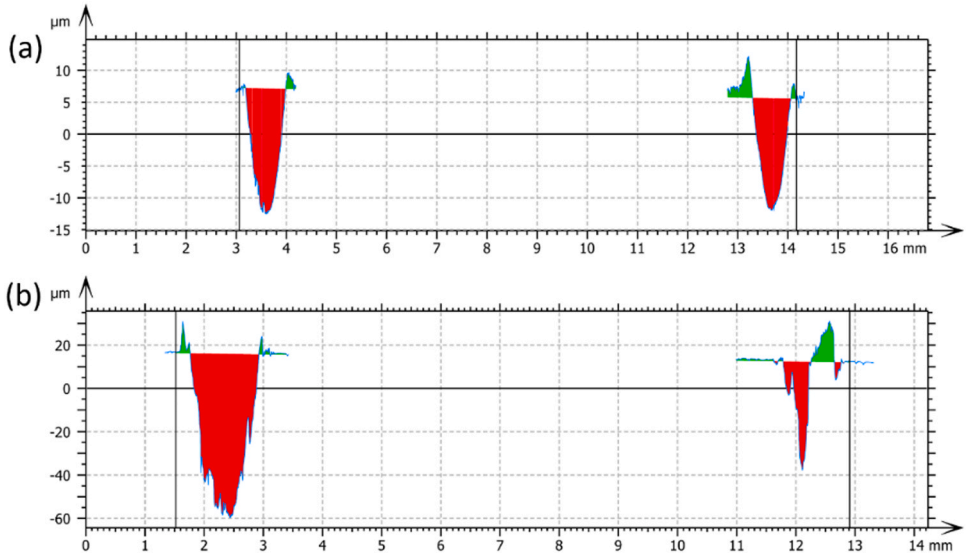

Fig. 8. Examples of measured profiles of (a) PTFE and (b) Aluminium. In red wear and in green galling volume contributions.

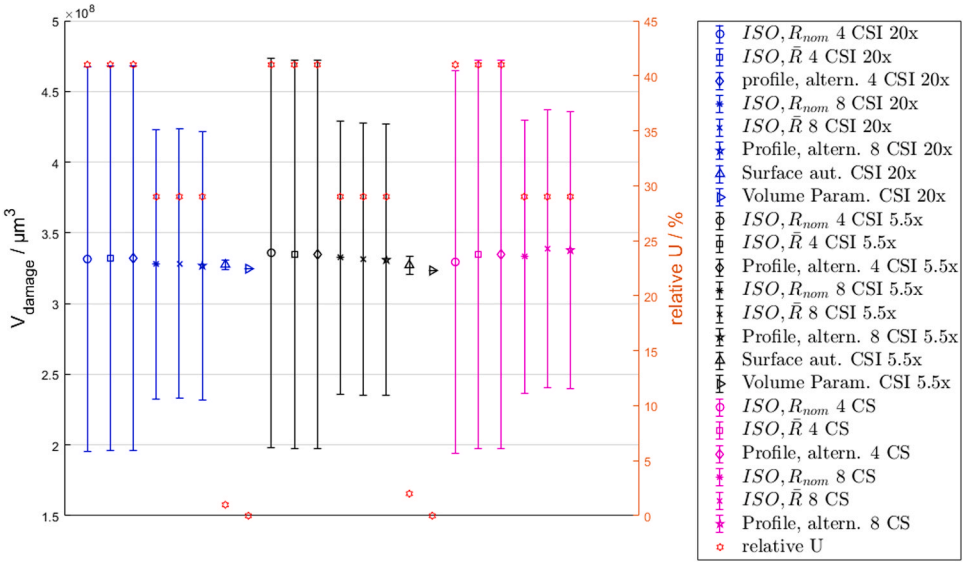

Fig. 9. Volume of total damage for PTFE sample (regular track). The legend reads according to Tables 8 and 9, where each legend entry specifies: the measurement method identification (*ISO* for standard profile-based method, *Profile altern* for alternative profile-based method, *Surface aut.* for automatic surface topography-based method implemented in MountainsMap, *Volume param.* for volume-parameters-based topographic method); the choice of the radius parameter (profile-based method only); the number of averaged profiles (profile-based method only); the overall instrument set-up.

an uneven track in which galling is not negligible (V_{wear} is 88% of the V_{damage}), as in the Aluminium case [74]. In a situation like this, the methods based on profiles extraction from topographical measurement can have up to 40% differences, which is partially compensated when a CS instrument is used due to the resolution effect. This affects the estimation of galling volume. The lateral resolution also impacts on the uncertainty as larger uncertainties are associated with coarser measurement methods.

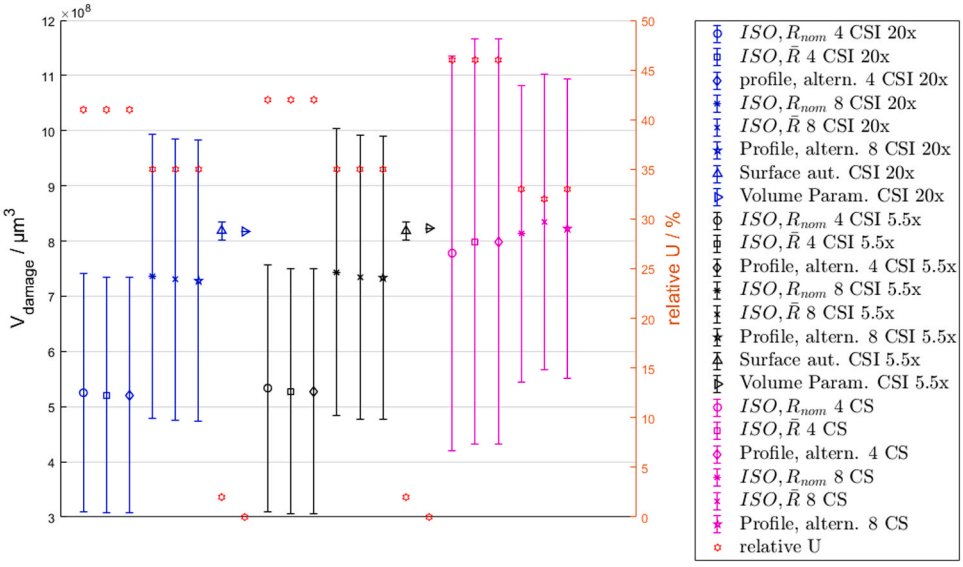

Fig. 10. Volume of total damage for Aluminium sample (uneven track). The legend reads according to Tables 8 and 9, where each legend entry specifies: the measurement method identification (*ISO* for standard profile-based method, *Profile altern* for alternative profile-based method, *Surface aut.* for automatic surface topography-based method implemented in MountainsMap, *Volume param.* for volume-parameters-based topographic method); the choice of the radius parameter (profile-based method only); the number of averaged profiles (profile-based method only); the overall instrument set-up.

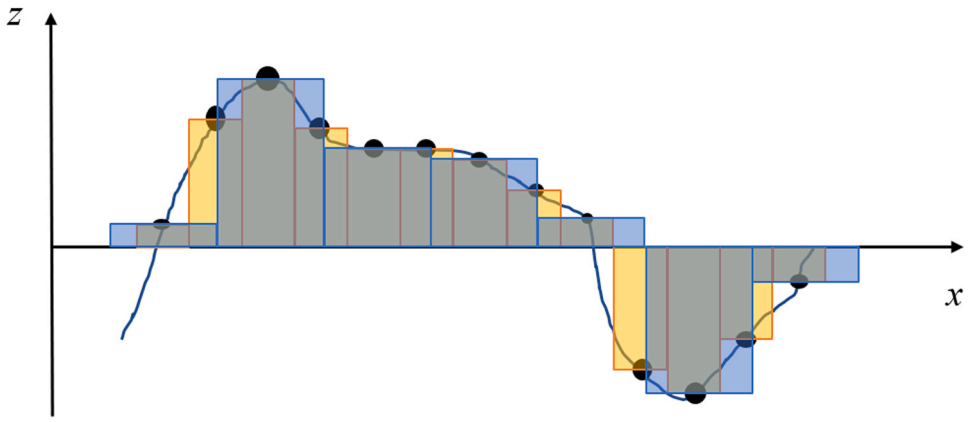

Fig. 11. Effect of lateral sampling resolution on the estimation of area. Coarser resolution (blue) overestimates areas.

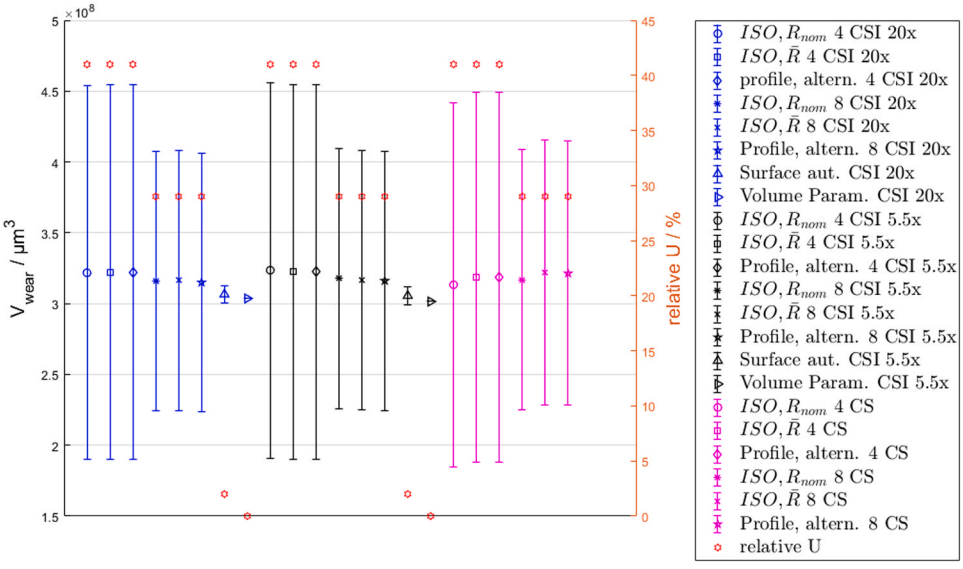

Fig. 12. Volume of wear for PTFE sample (regular track). The legend reads according to Tables 8 and 9, where each legend entry specifies: the measurement method identification (*ISO* for standard profile-based method, *Profile altern* for alternative profile-based method, *Surface aut.* for automatic surface topography-based method implemented in MountainsMap, *Volume param.* for volume-parameters-based topographic method); the choice of the radius parameter (profile-based method only); the number of averaged profiles (profile-based method only); the overall instrument set-up.

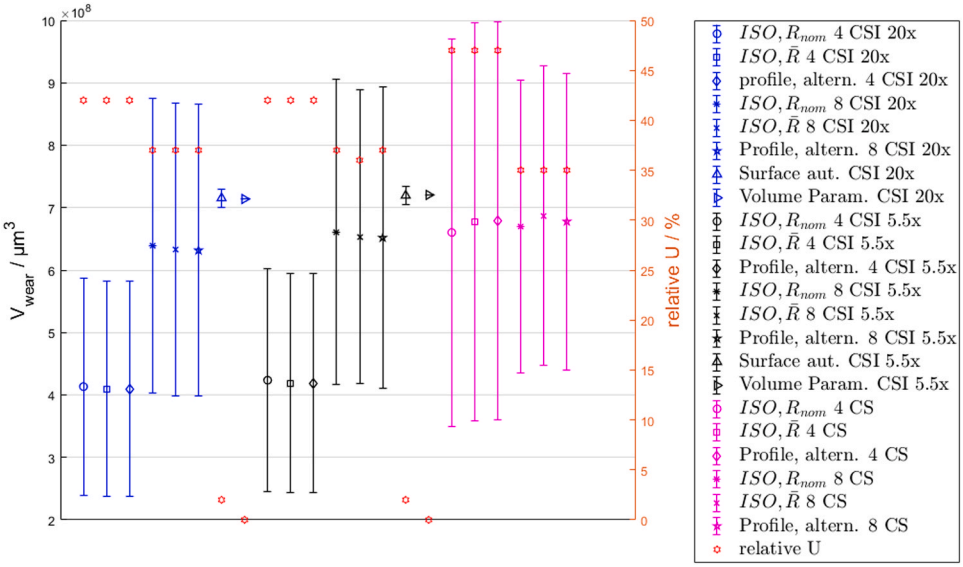

Fig. 13. Volume of wear for Aluminium sample (uneven track). The legend reads according to Tables 8 and 9, where each legend entry specifies: the measurement method identification (*ISO* for standard profile-based method, *Profile altern* for alternative profile-based method, *Surface aut.* for automatic surface topography-based method implemented in MountainsMap, *Volume param.* for volume-parameters-based topographic method); the choice of the radius parameter (profile-based method only); the number of averaged profiles (profile-based method only); the overall instrument set-up.

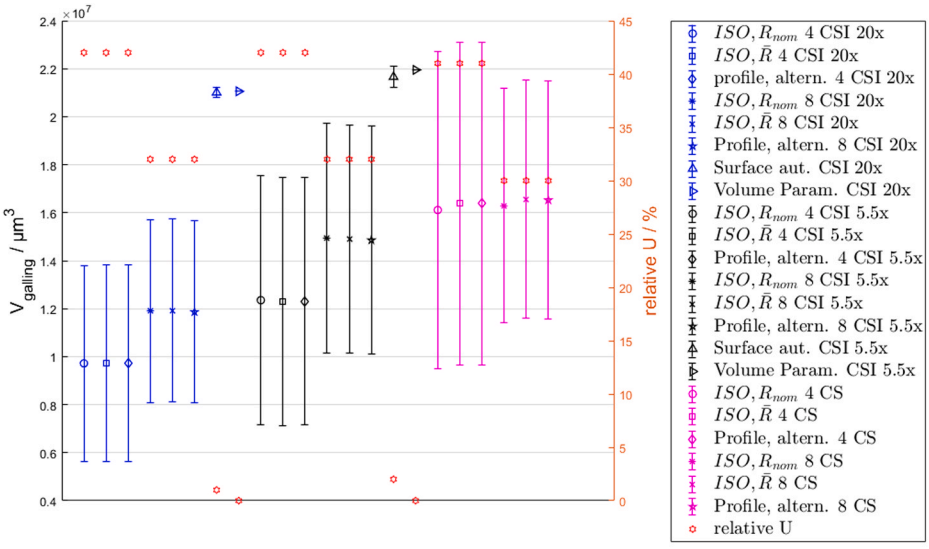

Fig. 14. Volume of galling for PTFE sample (regular track). The legend reads according to Tables 8 and 9, where each legend entry specifies: the measurement method identification (*ISO* for standard profile-based method, *Profile altern* for alternative profile-based method, *Surface aut.* for automatic surface topography-based method implemented in MountainsMap, *Volume param.* for volume-parameters-based topographic method); the choice of the radius parameter (profile-based method only); the number of averaged profiles (profile-based method only); the overall instrument set-up.

6. Conclusions

This work addressed the challenge of measuring wear in pin-on-disc tribological test, specifically measuring the damage on the flat disc. Current standards propose characterisation methods based on the measurement of the weight loss or the extraction of profiles from the wear tracks, but additional methods based on surface topography measurements are already available in the scientific literature. However, their performances in terms of measurement uncertainties are still unreported, which hinders from comparing the methods properly and reporting uncertainty of measured quantities. This paper evaluated the measurement uncertainties based on the current standardised framework of the metrological characteristics of surface topography measuring instruments. The developed theoretical framework was then exploited to compare the available methods within a metrological framework through a practical case study. The main findings and conclusions are summarised as follows:

A state-of-the-art framework to evaluate the uncertainty of wear volume measurements in the pin-on-disc test was developed.

- The method allows reporting the uncertainty of measured quantity, which is essential to compare the characterisation methods performances and to enable metrologically rigorous comparison of tested materials.
- Surface topography-based methods provide a thorough description of the phenomenon; they are regarded as the most informative and resulted in being the most precise, and they can be considered the state-of-the-art approach to implement the volumetric method.
- Standard methods based on sparse profiles measurement are affected by two issues. On the one hand, the measuring instrument's lateral resolution introduces systematic differences in the measured volume so that coarser measurement methods, like CS, tend to overestimate the wear volume. On the other hand, the extraction of few profiles generates criticalities concerning the representativeness and limits the capability of dealing with irregular tracks and localised phenomena.
- Contact Stylus measurement, i.e. the coarser measurement technique considered in this study, is not systematically different from other methods. i.e. its uncertainty bar overlaps to those of other methods, although at the cost of the worst measurement uncertainty.

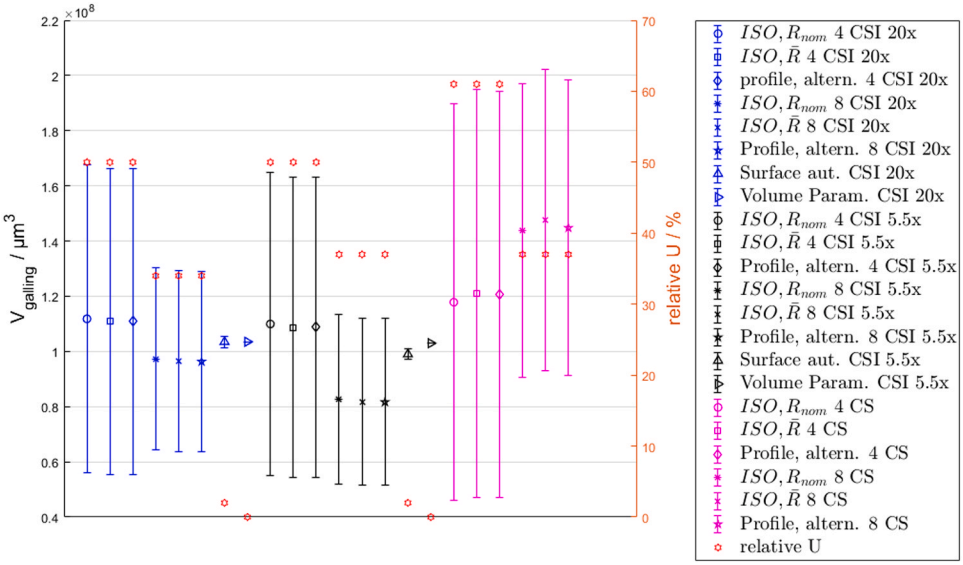

Fig. 15. Volume of galling for Aluminium sample (uneven track). The legend reads according to Tables 8 and 9, where each legend entry specifies: the measurement method identification (*ISO* for standard profile-based method, *Profile altern* for alternative profile-based method, *Surface aut.* for automatic surface topography-based method implemented in MountainsMap, *Volume param.* for volume-parameters-based topographic method); the choice of the radius parameter (profile-based method only); the number of averaged profiles (profile-based method only); the overall instrument set-up.

- Provided the shown higher precision and the known higher informativeness of surface topography-based methods, they shall be exploited to test calibration methods and performances of calibration materials for conventional model tests to establish a route for traceability for these wear measurement techniques.
- Although accuracy can be stated only in relative terms (because a 'true value' of wear volume is lacking), surface topography-based approaches were demonstrated to have the best metrological performances and robustness. If exploited for calibration, the surface topography-based methods will enable the evaluation of (absolute) accuracy of other characterisation approaches.
- The informativeness of the measurement approach affects the difference in accuracy amongst the characterisation methods. Sparser measurements, i.e. based on few profiles, are less representative of localised phenomena, e.g. galling in PTFE. In particular, this effect is dramatic for uneven wear tracks (Aluminium case), leading to differences between average values up to 60% in terms of total damage.
- Based on what was stated before, extracting a limited set of profiles, if a complete topography dataset is available, negatively affects the results because of the significant information loss. This approach common in literature should be discouraged, and tribological standards might consider including state-of-the-art surface topography measurement techniques.

The relative high uncertainty, i.e. low precision, that characterises the standard methods pose some questions regarding their suitability to measure wear volumes, especially very low wear volumes, which nowadays are more and more common in many cutting-edge tribological, e.g. innovative coatings, composites with ceramic reinforcements and lubrication-associated wear problems. The performance comparison of the available methods showed a systematic difference in the resulting estimated volume and their uncertainties. These differences, solely due to wear measurement approaches, may induce severe errors in characterising wear modes of materials and hamper the detection of meaningful wear behaviour changes.

Future works will exploit these results to improve the understanding of the main influence parameters on pin-on-disc wear measurements and may support the development of calibration standards and procedures to establish the traceability of the method. Future investigation will also address the challenges of the pin wear measurement through the developed methodology.

CRediT authorship contribution statement

Giacomo Maculotti: Conceptualization, Methodology, Software, Formal analysis, Investigation, Writing – original draft, Visualisation. **Edoardo Goti**: Conceptualization, Methodology, Investigation, Data curation, Writing – original draft. **Gianfranco Genta**: Conceptualization, Validation, Visualization, Writing – review & editing. **Luigi Mazza**: Term, Conceptualization, Writing – review & editing, Resources, Supervision. **Maurizio Galetto**: Funding Acquisition, Resources, Supervision.

Declaration of Competing Interest

The authors declare that they have no known competing financial interests or personal relationships that could have appeared to influence the work reported in this paper.

Acknowledgements

This work has been partially supported by "Ministero dell'Istruzione, dell'Università e della Ricerca", Award "TESUN-83486178370409 finanziamento dipartimenti di eccellenza CAP.1694 TIT. 232 ART. 600".

Annex A.

This annex reports computation detail to estimate the measurement uncertainty of the different approaches discussed in this paper.

A.1 Standard method

$$\overline{V_{ISO}} = \frac{2\pi}{N} d_x R \sum_{j=1}^{N\geq 4} \sum_{i=1}^{M} |z_{ji}| = \frac{2\pi}{N} R \sum_{j=1}^{N\geq 4} S_j = 2\pi R \overline{S} \tag{A.1}$$

First, the variance $u^2(S_j)$ can be evaluated according to its definition in Eqs. (3) and (9):

$$\boldsymbol{X} = \begin{bmatrix} d_x \\ \sum_i^M |z_i| \end{bmatrix} \tag{A.2.1}$$

$$\boldsymbol{c} = \begin{bmatrix} \sum_i^M |z_i| \\ d_x \end{bmatrix} \tag{A.2.2}$$

$$\boldsymbol{VCV} = \begin{bmatrix} u^2(d) & 0 \\ 0 & u^2\left(\sum_i^M |z_i|\right) \end{bmatrix}, \quad u^2\left(\sum_i^M |z_i|\right) = Mu^2(z) \tag{A.2.3}$$

$$u^2(S_j) = \left(\sum_i^M |z_i|\right)^2 u^2(d) + (d_x)^2 u^2\left(\sum_i^M |z_i|\right) = \left(\frac{S_j}{d_x}\right)^2 u^2(d) + d_x{}^2 M u^2(z) \tag{A.2.4}$$

from which the variance of the average cross-section follows:

$$\overline{S} = \frac{\sum_{j=1}^{N\geq 4} S_j}{N} \tag{A.3.1}$$

$$u^2\left(\overline{S}\right) = \frac{\sum_{j=1}^{N\geq 4} u^2(S_j)}{N^2} = \frac{\mathbb{E}\left[u^2(S_j)\right]}{N} \tag{A.3.2}$$

which is different from the variance of the sample mean, despite the definition of $\overline{S}$, because $u^2(S_j)$ depends on S_j (as shown in Eq.(A.2.4)).

Then the contribution *u(R)* due to the track radius *R* can be assessed. It depends on the choice of *R* between R_{nom} and $\overline{R}$. In the first case, u(R_{nom}) can be estimated according to the P.U.Ma. method as two units of the least significant digit of the mean value, 2•*LSD*, and associating to this half range a uniform distribution [62], so that its equivalent variance results in:

$$u^2(R_{nom}) = \frac{2 \bullet LSD}{3} \tag{A.4}$$

In the second case, the law of variance propagation has to be invoked, based on the definition of $\overline{R} = \frac{\sum_j^{N\geq 4} R_j}{N}$. As shown in Fig. 3, profiles are typically extracted in pairs along a given radial direction $\overrightarrow{r}$. Each measured pair identifies an external diameter D_{ext} and an internal diameter D_{in}, so that:

$$R_j = \frac{1}{2}\left(\frac{D_{ext,j} + D_{in,j}}{2}\right) \tag{A.5}$$

Therefore, it is necessary to express the coordinate change from cartesian coordinates *O(x,y)* to polar coordinates *O(r, ϑ)*:

$$\left\{ \begin{array}{l} r = x\cos\vartheta + y\sin\vartheta \\ \vartheta = \tan^{-1}\left(\frac{y}{x}\right) \end{array} \right\} \tag{A.6.1}$$

$$x = r\cos\vartheta \tag{A.6.2}$$

$$y = r\sin\vartheta \tag{A.6.3}$$

Since diameters are extracted along $\overrightarrow{r}$, the variance of the length *r* due to the change of coordinates can be computed:

$$\boldsymbol{X} = \begin{bmatrix} x \\ y \\ \vartheta \end{bmatrix} \tag{A.7.1}$$

$$\boldsymbol{c} = \begin{bmatrix} \cos\vartheta \\ \sin\vartheta \\ -x\sin\vartheta + y\cos\vartheta \end{bmatrix} = \begin{bmatrix} \cos\vartheta \\ \sin\vartheta \\ -r\cos\vartheta\sin\vartheta + r\sin\vartheta\cos\vartheta \end{bmatrix} = \begin{bmatrix} \cos\vartheta \\ \sin\vartheta \\ 0 \end{bmatrix} \tag{A.7.2}$$

$$\boldsymbol{VCV} = \begin{bmatrix} u^2(x) & 0 & 0 \\ 0 & u^2(y) & 0 \\ 0 & 0 & u^2(\vartheta) \end{bmatrix} \tag{A.7.3}$$

$$u^2(r) = u^2(x)\cos\vartheta^2 + u^2(y)\sin\vartheta^2 \tag{A.7.4}$$

Eq.(19.4) shows that the uncertainty of the length *r* along the direction ϑ depends on ϑ only and therefore $u^2(D_{ext}) = u^2(D_{in}) = u^2(D)$ because D_{ext} and D_{in} are measured along the same direction. It is thus possible to evaluate the variance of R_j, by the definition in Eq.(A.5):

$$\boldsymbol{X} = \begin{bmatrix} D_{ext} \\ D_{in} \end{bmatrix} \tag{A.8.1}$$

$$\boldsymbol{c} = \begin{bmatrix} 1/4 \\ 1/4 \end{bmatrix} \tag{A.8.2}$$

$$\boldsymbol{VCV} = \begin{bmatrix} u^2(D_{ext}) & 0 \\ 0 & u^2(D_{in}) \end{bmatrix} = \begin{bmatrix} u^2(D) & 0 \\ 0 & u^2(D) \end{bmatrix} \tag{A.8.3}$$

$$u^2(R_j) = \frac{2}{16}\left(u^2(x)\cos\vartheta^2 \quad + u^2(y)\sin\vartheta^2\right) \quad = \frac{1}{8}\left(u^2(x)\cos\vartheta^2 \quad + u^2(y)\sin\vartheta^2\right) \tag{A.8.4}$$

The evaluation of the variance of the average radius is computed based on Eq.(A.8.4):

$$\overline{R} = \frac{\sum_{j=1}^{N\geq 4} R_j}{N} \tag{A.9.1}$$

$$u^2\left(\overline{R}\right) = \frac{\sum_{j=1}^{N\geq 4} u^2(R_j)}{N^2} = \frac{\mathbb{E}\left[u^2(R_j)\right]}{N} \tag{A.9.2}$$

which is different from the variance of a sample mean because $u^2(R_j)$ depends on the extraction direction ϑ.

Finally, the variance of the standardised volumetric method for the mean wear volume measurement can be computed taking into account its definition in Eq. (2.2) and the contribution from the area of the average cross-section, Eq.(A.3), and from the track radius, for which two alternatives are possible:

$$\boldsymbol{X} = \begin{bmatrix} R \\ \overline{S} \end{bmatrix} \tag{A.10.1}$$

$$\boldsymbol{c} = \begin{bmatrix} 2\pi\overline{S} \\ 2\pi R \end{bmatrix} \tag{A.10.2}$$

$$\boldsymbol{VCV} = \begin{bmatrix} u^2(R) & 0 \\ 0 & u^2\left(\overline{S}\right) \end{bmatrix} \tag{A.10.3}$$

$$u^2\left(\overline{V_{ISO}}\right) = 4\pi^2\left(\overline{S}^2 u^2(R) + \quad R^2 u^2\left(\overline{S}\right)\right) \tag{A.10.4}$$

The latter equation can be rewritten by outlining explicitly the two possible way to handle R:

$$u^2\left(\overline{V_{ISO,R_{nom}}}\right) = 4\pi^2\left(\overline{S}^2 u^2(R_{nom}) + \quad {R_{nom}}^2\frac{\mathbb{E}\left[u^2(S_j)\right]}{N}\right) \tag{A.11}$$

$$u^2\left(\overline{V_{ISO,\overline{R}}}\right) = \frac{4\pi^2}{N}\left(\overline{S}^2\mathbb{E}\left[u^2(R_j)\right] + \quad \overline{R}^2\mathbb{E}\left[u^2(S_j)\right]\right) \tag{A.12}$$

A.2 Alternative method based on profile extraction

$$\overline{V_{prof,\ \ alt}} = \frac{2\pi}{N}\sum\nolimits_j^{N\geq 4} R_j S_j = 2\pi\overline{RS} \tag{A.13}$$

It is first estimated $u^2(R_jS_j)$:

$$\boldsymbol{X} = \begin{bmatrix} R_j \\ S_j \end{bmatrix} \tag{A.14.1}$$

$$\boldsymbol{c} = \begin{bmatrix} S_j \\ R_j \end{bmatrix} \tag{A.14.2}$$

$$\boldsymbol{VCV} = \begin{bmatrix} u^2(R_j) & 0 \\ 0 & u^2(S_j) \end{bmatrix} \tag{A.14.3}$$

$$u^2(R_jS_j) = {S_j}^2 u^2(R_j) + {R_j}^2 u^2(S_j) \tag{A.14.4}$$

from which $u^2\left(\overline{RS}\right)$ can now be written as:

$$u^2\left(\overline{RS}\right) = \frac{\sum_{j=1}^{N\geq 4} u^2(R_jS_j)}{N^2} = \frac{\mathbb{E}\left[u^2(R_jS_j)\right]}{N} \tag{A.15}$$

that allows to write the wanted result:

$$u^2\left(\overline{V_{prof,\ \ alt}}\right) = 4\pi^2 u^2\left(\overline{RS}\right) = 4\pi^2\frac{\mathbb{E}\left[u^2(R_jS_j)\right]}{N} \tag{A.16}$$

A.3 Automatic surface topography-based method

$$V_{aut} = d_y \sum_{j=2}^{N-1} S_j + \frac{d_y}{2}(S_1 + S_N) \tag{A.17}$$

Provided the evaluation of $u^2(S_j)$ in Eq.(A.2.4), it can be written:

$$\boldsymbol{X} = \begin{bmatrix} S_1 \\ S_N \\ S_j \\ d_y \end{bmatrix} \tag{A.18.1}$$

$$\boldsymbol{c} = \begin{bmatrix} d_y/2 \\ d_y/2 \\ d_y \\ \sum_{j=2}^{N-1} S_j + \dfrac{S_1 + S_N}{2} \end{bmatrix} \tag{A.18.2}$$

$$\boldsymbol{VCV} = \begin{bmatrix} u^2(S_1) & 0 & 0 & 0 \\ 0 & u^2(S_2) & 0 & 0 \\ 0 & 0 & u^2(S_j) & 0 \\ 0 & 0 & 0 & u^2(d) \end{bmatrix} \tag{A.18.3}$$

$$u^2(V_{aut}) = \frac{d_y^2}{4}\left(u^2(S_1) + u^2(S_N)\right) + d_y^2 \sum_{j=2}^{N-1} u^2(S_j) \quad + \left(\sum_{j=2}^{N-1} S_j + \frac{S_1 + S_N}{2}\right)^2 u^2(d) \tag{A.18.4}$$

A.4 Volume parameter method

$$V_m(m_r) = \quad K \sum_{j=1}^{B} \Delta z_j m_{rj} \tag{A.19.1}$$

$$V_v(m_r) = K\left(100\%(z_{max} - h) - \sum_{j=B+1}^{N_{bin}} \Delta z_j m_{rj}\right) \tag{A.19.2}$$

$$K = n_x n_y d^2 \tag{A.19.3}$$

First of all, the variance of K can be computed as:

$$\boldsymbol{X} = [d] \tag{A.20.1}$$

$$\boldsymbol{c} = \left[2dn_x n_y\right] \tag{A.20.2}$$

$$\boldsymbol{VCV} = \left[u^2(d)\right] \tag{A.20.3}$$

$$u^2(K) = 4 \bullet \left(\mathrm{n_x n_y}\right)^2 \bullet \mathrm{d}^2 \bullet \mathrm{u}^2(\mathrm{d}) = 4\mathrm{K n_x n_y u}^2(\mathrm{d}) \tag{A.20.4}$$

Then, the variance of V_m, i.e. the $V_{gallling}$, is computed:

$$\boldsymbol{X} = \begin{bmatrix} K \\ \Delta z_j \end{bmatrix} \tag{A.21.1}$$

$$\boldsymbol{c} = \begin{bmatrix} \sum_{j=1}^{B} \Delta z_j \, m_{rj} \\ K m_{rj} \end{bmatrix} \tag{A.21.2}$$

$$\boldsymbol{VCV} = \begin{bmatrix} u^2(K) & 0 \\ 0 & 2u^2(z) \end{bmatrix} \tag{A.21.3}$$

$$u^2(V_m(m_r)) = \left(\sum_{j=1}^{B} \Delta z_j m_{rj}\right)^2 u^2(K) + 2K^2 \sum_{j=1}^{B} m_{rj}^2 u^2(z) \tag{A.21.4}$$

Similarly, the variance of V_v, i.e. the V_{wear}, results from:

$$\boldsymbol{X} = \begin{bmatrix} K \\ z_{max} - h \\ \Delta z_j \end{bmatrix} \tag{A.22.1}$$

$$\boldsymbol{c} = \begin{bmatrix} \left((z_{max} - h) - \sum_{j=B+1}^{N_{bin}} \Delta z_j \, m_{r_j}\right) \\ K \\ -K m_{r_j} \end{bmatrix} \tag{A.22.2}$$

$$\boldsymbol{VCV} = \begin{bmatrix} u^2(K) & 0 & 0 \\ 0 & 2u^2(z) & 0 \\ 0 & 0 & 2u^2(z) \end{bmatrix} \tag{A.22.3}$$

$$u^2(V_v(m_r)) = \left((z_{max} - h) - \sum_{j=B+1}^{N_{bin}} \Delta z_j m_{r_j}\right)^2 u^2(K) + 2K^2\left(1 + \sum_{j=B+1}^{N_{bin}} m_{r_j}^2\right) u^2(z) \tag{A.22.4}$$

Last, if the total damage is of interest, and consequently its variance, the last two results can be combined so that it results:

$$u^2(V_{VP}) = u^2(V_m(m_r)) + u^2(V_v(m_r)) \tag{A.23.1}$$

$$u^2(V_{VP}) = \left[\left(\sum_{j=1}^{B} \Delta z_j m_{r_j}\right)^2 + \left((z_{max} - h) - \sum_{j=B+1}^{N_{bin}} \Delta z_j m_{r_j}\right)^2\right] u^2(K) + 2K^2\left[1 + \sum_{j=1}^{N_{bin}} m_{r_j}^2\right] u^2(z) \tag{A.23.2}$$

$$u^2(V_{VP}) = \left[\left(\frac{V_m(m_r)}{K}\right)^2 + \left(\frac{V_v(m_r)}{K}\right)^2\right] u^2(K) + 2K^2\left[1 + \sum_{j=1}^{N_{bin}} m_{r_j}^2\right] u^2(z) \tag{A.23.3}$$

References

[1] Whitenton EP, Blau PJ. A comparison of methods for determining wear volumes and surface parameters of spherically tipped sliders. Wear 1988;124:291–309.
[2] Zum Gahr K-H. Microstructure and Wear of Materials. Elsevier; 1987.
[3] Zhang X, Yu T, Dai Y, Qu S, Zhao J. P7C3-A20 alleviates fatty liver by shaping gut microbiota and inducing FGF21/FGF1, via the AMP-activated protein kinase/CREB regulated transcription coactivator 2 pathway. Br J Pharm 2021;178:2111–30.
[4] Straffelini G. Friction and Wear Methodologies for Design and Control. Springer; 2015.
[5] Bhushan B. Modern Tribology Handbook. CRC Press; 2000.
[6] Blau PJ. Friction Science and Technology: From Concepts to Applications. Boca Ranton, FL (USA): CRC Press; 2008.
[7] Peng LF, Mao MY, Fu MW, Lai XM. Effect of grain size on the adhesive and ploughing friction behaviours of polycrystalline metals in forming process. Int J Mech Sci 2016;117:197–209.
[8] Stachowiak GW, Batchelor AW. Engineering Tribology. Oxford: Butterworth-Heinemann; 2008.
[9] Joseph J, Haghdadi N, Shamlaye K, Hodgson P, Barnett M, Fabijanic D. The sliding wear behaviour of CoCrFeMnNi and AlxCoCrFeNi high entropy alloys at elevated temperatures. Wear 2019;428–429:32–44.
[10] An J, Sun W, Niu XD. Dry sliding wear behavior and a proposed criterion for mild to severe wear transition of Mg–3Al–0.4Si–0.1Zn alloy. Tribol Lett 2017;65:98.
[11] Madhukar P, Selvaraj N, Rao CSP, Veeresh Kumar GB. Fabrication and characterization two step stir casting with ultrasonic assisted novel AA7150-hBN nanocomposites. J Alloy Compd 2020;815:152464.
[12] Baran Ö, Keleş A, Çiçek H, Totik Y, Efeoğlu İ. The mechanical and tribological properties of Ti [Nb, V] N films on the Al-2024 alloy. Surf Coat Technol 2017;332:312–8.
[13] Mura A, Wang H, Adamo F, Kong J. Graphene coatings to enhance tribological performance of steel. Mech Adv Mater Struct 2019;28:657–64.
[14] Mura A, Canavese G, Goti E, Rivolo P, Wang H, Ji X, et al. Effect of different types of graphene coatings on friction and wear performance of aluminum alloy. Mech Adv Mater Struct 2020:1–9.
[15] long Liu X, bing Cai Z, xiao Q, xue Shen M, bin Yang W, yun Chen D. Fretting wear behavior of brass/copper-graphite composites as a contactor material under electrical contact. Int J Mech Sci 2020;184:105703.
[16] Salguero J, Vazquez-Martinez JM, Del Sol I, Batista M. Application of Pin-On-Disc techniques for the study of tribological interferences in the dry machining of A92024-T3 (Al-Cu) alloys. Materials, 11. Basel,; 2018. p. 1–11.
[17] Zappelino BF, dos EA, de Almeida S, Krelling AP, da Costa CE, Fontana LC, et al. Tribological behavior of duplex-coating on Vanadis 10 cold work tool steel. Wear 2020;442–443:203133.
[18] Verna E, Biagi R, Kazasidis M, Galetto M, Bemporad E, Lupoi R. Modeling of erosion response of cold-sprayed In718-Ni composite coating using full factorial design. Coatings 2020;10:335.
[19] Kovacı H. Comparison of the microstructural, mechanical and wear properties of plasma oxidised Cp-Ti prepared by laser powder bed fusion additive manufacturing and forging processes. Surf Coat Technol 2019;374:987–96.
[20] Norani MNM, Bin Abdollah MF, Abdullah MIHC, Amiruddin H, Ramli FR, Tamaldin N. 3D printing parameters of acrylonitrile butadiene styrene polymer for friction and wear analysis using response surface methodology. Proc Inst Mech Eng Part J J Eng Tribol 2020. 1350650120925601.
[21] Müller M, Ostermeyer G-P. Measurements of partially lubricated contacts on different scales. PAMM 2017;17:629–30.
[22] Elwasli F, Mzali S, Zemzemi F, Mkaddem A, Mezlini S. Effects of initial surface topography and contact regimes on tribological behavior of AISI-52100/AA5083 materials' pair when reciprocating sliding. Int J Mech Sci 2018;137:271–83.
[23] Wang X, Zhang Y, Yin Z, Su Y, Zhang Y, Cao J. Experimental research on tribological properties of liquid phase exfoliated graphene as an additive in SAE 10W-30 lubricating oil. Tribol Int 2019;135:29–37.
[24] Kerni L, Raina A, Haq MIU. Friction and wear performance of olive oil containing nanoparticles in boundary and mixed lubrication regimes. Wear 2019;426–427:819–27.
[25] ASTM G99–17 Standard Test Method for Wear Testing with a Pin-on-Disk Apparatus.
[26] Bolelli G, Cannillo V, Lusvarghi L, Manfredini T. Wear behaviour of thermally sprayed ceramic oxide coatings. Wear 2006;261:1298–315.
[27] Miyoshi K, Ishibashi K, Suzuki M. Surface characterisation techniques in wear of materials. ASTM Spec Tech Publ 1501 STP 2008:126–33.
[28] Bolelli G, Rauch J, Cannillo V, Killinger A, Lusvarghi L, Gadow R. Microstructural and tribological investigation of high-velocity suspension flame sprayed (HVSFS) Al 2O 3 coatings. J Therm Spray Technol 2009;18:35–49.
[29] Hu B, Peng L, Yang Y, Ding W. Effect of solidification conditions on microstructure, mechanical and wear properties of Mg-5Al-3Ca-0.12Sr magnesium alloy. Mater Des 2010;31:3901–7.
[30] Lahiri D, Benaduce AP, Rouzaud F, Solomon J, Keshri AK, Kos L, et al. Wear behavior and in vitro cytotoxicity of wear debris generated from hydroxyapatite-carbon nanotube composite coating. J Biomed Mater Res - Part A 2011;96 A:1–12.
[31] Bao M, Zhang C, Lahiri D, Agarwal A. The tribological behavior of plasma-sprayed Al-Si composite coatings reinforced with nanodiamond. Jom 2012;64:702–8.
[32] Lahiri D, Gill PK, Scudino S, Zhang C, Singh V, Karthikeyan J, et al. Cold sprayed aluminum based glassy coating: synthesis, wear and corrosion properties. Surf Coat Technol 2013;232:33–40.
[33] Chung I, Lee S, do Kwon J. Fretting wear volume calculation on cylindrical surface: Inaccuracy due to misalignment of measured object with respect to 3D profiler. Wear 2013;297:1074–80.
[34] Sharma S, Sangal S, Mondal K. On the optical microscopic method for the determination of ball-on-flat surface linearly reciprocating sliding wear volume. Wear 2013;300:82–9.
[35] Dong R, Zhu W, Zhao C, Zhang Y, Ren F. Microstructure, mechanical properties, and sliding wear behavior of spark plasma sintered Ti-Cu alloys. Metall Mater Trans A Phys Metall Mater Sci 2018;49:6147–60.
[36] Türedi E. On the precise measurement capability of the direct microscopic measurement method for wear volume characterization. MATEC Web Conf 2018;188:02007.
[37] ASTM G40–17 Standard Terminology Relating to Wear and Erosion.
[38] Blau PJ. Tribosystem Analysis: A Practical Approach to the Diagnosis of Wear Problems A Practical Approach to the Diagnosis of Wear Problems. 2nd ed..,. Boca Ranton, FL (USA): CRC Press; 2016.
[39] Bayer RG. Mechanical Wear Fundamental and Testing. New York, NY, USA: Marcel Dekker Inc.; 2004.

[40] Wood FW. Summary on the role and analysis of wear in failures. J Test Eval 1994; 22:470–3.
[41] Fillot N, Iordanoff I, Berthier Y. Wear modeling and the third body concept. Wear 2007;262:949–57.
[42] Neale MJ, Gee M. A guide to Wear Problems and Testing for Industry. William Andrew Publishing; 2001.
[43] Aksulu M, Palabiyik M. Uncertainty of wear rate and coefficient of friction for a polymer wear experiment in a pad-on-disc tribotester. Proc 9th Bienn ASME Conf Eng Syst Des Anal 2008:451–6.
[44] D'Amato R, Calvo R, Ruggiero A, Gómez E. Measurement capabilities for ball bearing wear assessment. Procedia Manuf 2017;13:647–54.
[45] Wang QJ, Chung Y. Encyclopedia of Tribology. Boston, USA: Springer; 2013.
[46] ISO 18535-2. Diamond-like Carbon Films – Determination of Friction and Wear Characteristics of Diamond-like Carbon Films by Ball-on-disc Method. Genève: ISO; 2016.
[47] Leach RK. Characterisation of Areal Surface Texture. Berlin: Springer; 2013.
[48] Colbert RS, Krick BA, Dunn AC, Vail JR, Argibay N, Sawyer WG. Uncertainty in pin-on-disk wear volume measurements using surface scanning techniques. Tribol Lett 2011;42:129–31.
[49] Fleming GJP, Reilly E, Dowling AH, Addison O. Data acquisition variability using profilometry to produce accurate mean total volumetric wear and mean maximum wear depth measurements for the OHSU oral wear simulator. Dent Mater 2016;32: e176–84.
[50] Maculotti G, Goti E, Genta G, Marchiandi G, Mura A, Mazza L, et al. Effect of track geometry on the measurement uncertainty of wear in pin-on-disc tribological test. Proc 21st Int Conf Exhib EUSPEN 2021 (in press).
[51] Burris DL, Sawyer WG. Measurement uncertainties in wear rates. Tribol Lett 2009; 36:81–7.
[52] Leach R. Characterisation of areal surface texture. Character Area Surf Texture 2013. https://doi.org/10.1007/978-3-642-36458-7.
[53] ISO 25178-2. Geometrical Product Specifications (GPS) – Surface Texture: Areal. Part 2: Terms, Definitions and Surface Texture Parameters. Genève: ISO; 2012.
[54] Takimoto RY, de Sales Guerra Tsuzuki M, Ueda EK, Sato AK, de Castro Martins T, Cousseau T, et al. Rough surface wear analysis using image processing. Tech, IFAC-Pap 2016;49:7–12.
[55] Carmignato S, Spinelli M, Affatato S, Savio E. Uncertainty evaluation of volumetric wear assessment from coordinate measurements of ceramic hip joint prostheses. Wear 2011;270:584–90.
[56] Valigi MC, Logozzo S, Affatato S. New challenges in tribology: wear assessment using 3D optical scanners. Materials, 10. Basel; 2017. p. 1–13.
[57] Genta G, Maculotti G. Uncertainty evaluation of small wear measurements on complex technological surfaces by machine vision-aided topographical methods. CIRP Ann 2021;70:451–4.
[58] Green NC, Bowen J, Hukins DWL, Shepherd DET. Assessment of non-contacting optical methods to measure wear and surface roughness in ceramic total disc replacements. Proc Inst Mech Eng Part H J Eng Med 2015;229:245–54. https://doi.org/10.1177/0954411915577119.
[59] Niemczewska-Wójcik M, Mańkowska-Snopczyńska A, Piekoszewski W. The investigation of wear tracks with the use of noncontact measurement methods. Arch Civ Mech Eng 2013;13:158–67.
[60] Waterworth A. Quantitative Characterisation of Surface Finishes on Stainless Steel Sheet using 3D Surface Topography Analysis. University of Huddersfield; 2006.
[61] Baryshev SV, Erck RA, Moore JF, Zinovev AV, Tripa CE, Veryovkin IV. Characterisation of surface modifications by white light interferometry: applications in ion sputtering, laser ablation, and tribology experiments. J Vis Exp M 2013:1–16.
[62] JCGM100. Evaluation of Measurement Data – Guide to the Expression of Uncertainty in Measurement (GUM). Sèvres, France: JCGM; 2008.
[63] ISO 25178-600. Geometrical Product Specification (GPS) – Surface Texture: Areal Part 600: Metrological Characteristics for Areal-Topography Measuring Methods. Genève: ISO; 2019.
[64] Leach RK. Optical Measurement of Surface Topography. Berlin: Springer; 2011.
[65] Giusca CL, Leach RK, Helary F, Gutauskas T, Nimishakavi L. Calibration of the scales of areal surface topography measuring instruments: part 2. Amplification, linearity and squareness. Meas Sci Technol 2012;23:065005.
[66] Giusca CL, Leach RK, Helery F. Calibration of the scales of areal surface topography measuring instruments: Part 2. Amplification, linearity and squareness. Meas Sci Technol 2012;23:065005.
[67] Giusca CL, Leach RK. Calibration of the scales of areal surface topography measuring instruments: part 3. Resolution. Meas Sci Technol 2013;24:105010.
[68] Leach RK, Haitjema H, Su R, Thompson A. Metrological characteristics for the calibration of surface topography measuring instruments: a review. Meas Sci Technol 2021;32:032001.
[69] Giusca CL, Claverley JD, Sun W, Leach RK, Helmli F, Chavigner MPJ. Practical estimation of measurement noise and flatness deviation on focus variation microscopes. CIRP Ann - Manuf Technol 2014;63:545–8.
[70] Alburayt A, Syam WP, Leach R. Lateral scale calibration for focus variation microscopy. Meas Sci Technol 2018;29:065012.
[71] Maculotti G, Feng X, Galetto M, Leach R. Noise evaluation of a point autofocus surface topography measuring instrument. Meas Sci Technol 2018;29:065008.
[72] Maculotti G, Feng X, Su R, Galetto M, Leach R. Residual flatness and scale calibration for a point autofocus surface topography measuring instrument. Meas Sci Technol 2019;30:075005.
[73] Weckenmann A, Tan O, Hoffmann J, Sun Z. Practice-oriented evaluation of lateral resolution for micro- and nanometre measurement techniques. Meas Sci Technol 2009;20:065103.
[74] Maculotti G. Advanced methods for the mechanical and topographical characterisation of technological surfaces. Politec di Torino 2021.